ATP6V0C variants impair vacuolar V-ATPase causing a neurodevelopmental disorder often associated with epilepsy

Kari A. Mattison,[1,2,†] Gilles Tossing,[3,†] Fred Mulroe,[4] Callum Simmons,[4] Kameryn M. Butler,[2,5] Alison Schreiber,[6] Adnan Alsadah,[6] Derek E. Neilson,[7,8] Karin Naess,[9,10] Anna Wedell,[9,11] Anna Wredenberg,[9,10] Arthur Sorlin,[12] Emma McCann,[13] George J. Burghel,[14] Beatriz Menendez,[15] George E. Hoganson,[16] Lorenzo D. Botto,[17] Francis M. Filloux,[18] Ángel Aledo-Serrano,[19] Antonio Gil-Nagel,[19] Katrina Tatton-Brown,[20] Nienke E. Verbeek,[21] Bert van der Zwaag,[21] Kyrieckos A. Aleck,[7,8] Andrew C. Fazenbaker,[8] Jorune Balciuniene,[22,23] Holly A. Dubbs,[24] Eric D. Marsh,[24] Kathryn Garber,[2] Jakob Ek,[25] Morten Duno,[25] Christina E. Hoei-Hansen,[26,27] Matthew A. Deardorff,[28,29,30] Gordana Raca,[28,30] Catherine Quindipan,[31] Michele van Hirtum-Das,[29,30] Jeroen Breckpot,[32] Trine Bjørg Hammer,[33] Rikke S. Møller,[33,34] Andrea Whitney,[35] Andrew G. L. Douglas,[36,37] Mira Kharbanda,[37] Nicola Brunetti-Pierri,[38,39] Manuela Morleo,[38,40] Vincenzo Nigro,[38,40] Halie J. May,[41] James X. Tao,[42] Emanuela Argili,[43,44] Elliot H. Sherr,[43,44] William B. Dobyns,[45] Genomics England Research Consortium,[46] Richard A. Baines,[4] Jim Warwicker,[47] J. Alex Parker,[3] Siddharth Banka,[48,‡] Philippe M. Campeau[49,‡] and Andrew Escayg[2,‡]

[†,‡]**These authors contributed equally to this work.**

1 Genetics and Molecular Biology Graduate Program, Graduate Division of Biological and Biomedical Sciences, Laney Graduate School, Emory University, Atlanta, GA, USA
2 Department of Human Genetics, Emory University, Atlanta, GA, USA
3 Department of Neuroscience, University of Montreal, Montreal, QC, Canada
4 Division of Neuroscience and Experimental Psychology, School of Biological Sciences, Faculty of Biology, Medicine and Health, University of Manchester, Manchester Academic Health Science Center, Manchester, UK
5 Greenwood Genetics Center, Greenwood, SC, USA
6 Center for Personalized Genetic Healthcare, Cleveland Clinic, Cleveland, OH, USA

7 Division of Genetics and Metabolism, Department of Child Health, The University of Arizona College of Medicine, Phoenix, AZ, USA
8 Department of Genetics and Metabolism, Phoenix Children's Hospital, Phoenix Children's Medical Group, Phoenix, AZ, USA
9 Center for Inherited Metabolic Diseases, Karolinska University Hospital, Stockholm, Sweden
10 Department of Medical Biochemistry and Biophysics, Karolinska Institute, Stockholm, Sweden
11 Deparment of Molecular Medicine and Surgery, Karolinska Institute, Stockholm, Sweden
12 National Center of Genetics, Laboratoire national de santé, Dudelange, Luxembourg
13 Liverpool Center for Genomic Medicine, Liverpool Women's Hospital, Liverpool, UK
14 Genomic Diagnostic Laboratory, St. Mary's Hospital, Manchester University NHS Foundation Trust, Manchester, UK
15 UI Health, Chicago, IL, USA
16 Division of Genetics, Department of Pediatrics, University of Illinois College of Medicine, Chicago, IL, USA
17 Division of Medical Genetics, Department of Pediatrics, University of Utah School of Medicine, Salt Lake City, UT, USA
18 Division of Pediatric Neurology, Department of Pediatrics, University of Utah School of Medicine, Salt Lake City, UT, USA
19 Genetic Epilepsy Program, Department of Neurology, Ruber International Hospital, Madrid, Spain
20 Medical Genetics, St. George's University Hospitals NHS Foundation Trust and Institute for Molecular and Cell Sciences, St. George's, University of London, London, UK
21 Department of Genetics, University Medical Center Utrecht, Member of the ERN EpiCARE, Utrecht, The Netherlands
22 Divison of Genomic Diagnostics, Department of Pathology and Laboratory Medicine, Children's Hospital of Philadelphia, Philadelphia, PA, USA
23 PerkinElmer Genomics, Pittsburgh, PA, USA
24 Division of Neurology, Children's Hospital of Philadelphia, Philadelphia, PA, USA
25 Department of Clinical Genetics, University Hospital of Copenhagen, Copenhagen, Denmark
26 Department of Pediatrics, University Hospital of Copenhagen, Copenhagen, Denmark
27 Department of Clinical Medicine, University of Copenhagen, Copenhagen, Denmark

28 Department of Pathology and Laboratory Medicine, Children's Hospital Los Angeles, Los Angeles, CA, USA
29 Department of Pediatrics, Division of Medical Genetics, Children's Hospital Los Angeles, Los Angeles, CA, USA
30 Keck School of Medicine, University of Southern California, Los Angeles, CA, USA
31 Center for Personalized Medicine, Children's Hospital Los Angeles, Los Angeles, CA, USA
32 Center for Human Genetics, University Hospitals Leuven, Leuven, Belgium
33 Department of Epilepsy Genetics and Personalized Medicine, Danish Epilepsy Center, Fildelfia, Dianalund, Denmark
34 Insititue for Regional Health Services Research, University of Southern Denmark, Odense, Denmark
35 Pediatric Neurology, University Hospital Southampton NHS Foundation Trust, Southampton, UK
36 Wessex Clinical Genetics Service, University of Southampton, Southampton, UK
37 Human Development and Health, Faculty of Medicine, University of Southampton, Southampton, UK
38 Telethon Institute of Genetics and Medicine (TIGEM), Pozzuoli, Italy
39 Department of Translational Medicine, Federico II University of Naples, Naples, Italy
40 Department of Precision Medicine, University of Campania 'Luigi Vanvitelli', Naples, Italy
41 Institute for Genomic Medicine, Columbia University Irving Medical Center, New York, NY, USA
42 Department of Neurology, University of Chicago, Chicago, IL, USA
43 Department of Neurology, University of California, San Francisco, San Francisco, CA, USA
44 Pediatrics Institute of Human Genetics and Weill Institute for Neurosciences, University of California, San Francisco, San Francisco, CA, USA
45 Department of Pediatrics, Division of Genetics and Metabolism, University of Minnesota, Minneapolis, MN, USA
46 Genomics England and William Harvey Research Institute, Queen Mary University of London, London, UK
47 School of Biological Sciences, Faculty of Biology, Medicine and Health, Manchester Institute of Biotechnology, University of Manchester, UK

48 Division of Evolution, Infection, and Genomics, School of Biological Sciences, Faculty of Biology, Medicine and Health, University of Manchester, Manchester, UK
49 Department of Pediatrics, University of Montreal, Montreal, QC, Canada

Correspondence to: Andrew Escayg
Department of Human Genetics
Emory University
615 Michael Street
Atlanta, GA 30322
E-mail: aescayg@emory.edu

Correspondence may also be addressed to: Philippe M. Campeau
Department of Pediatrics
University of Montreal
Montreal, QC, Canada
E-mail: p.campeau@umontreal.ca

Siddharth Banka
University of Manchester
Manchester, UK
E-mail: Siddharth.banka@manchester.ac.uk

Running title: *ATP6V0C* variants impair V-ATPase activity

Keywords: V-ATPase; ATP6V0C; VMA3; epilepsy genetics; neurodevelopmental disorders

Abbreviations: eAUC = empirical area under the curve; gnomAD = genome aggregation database; NMD = nonsense mediated decay; SV = synaptic vesicle

Abstract

The vacuolar H^+-ATPase (V-ATPase) is an enzymatic complex that functions in an ATP-dependent manner to pump protons across membranes and acidify organelles, thereby creating the proton/pH gradient required for membrane trafficking by several different types of transporters. We describe heterozygous point variants in *ATP6V0C*, encoding the c-subunit in the membrane bound integral domain of the V-ATPase, in 27 patients with neurodevelopmental abnormalities with or without epilepsy. Corpus callosum hypoplasia and cardiac abnormalities were also present in some patients. *In silico* modeling suggested that the patient variants interfere with the interactions between the ATP6V0C and ATP6V0A subunits during ATP hydrolysis. Consistent with decreased V-ATPase activity, functional analyses conducted in *Saccharomyces cerevisiae* revealed reduced LysoSensor fluorescence and reduced growth in media containing varying concentrations of $CaCl_2$. Knockdown of ATP6V0C in Drosophila resulted in increased duration of seizure-like behavior, and the expression of selected patient variants in *Caenorhabditis elegans* led to reduced growth, motor dysfunction, and reduced lifespan. In summary, this study establishes *ATP6V0C* as an important disease gene, describes the clinical features of the associated neurodevelopmental disorder, and provides insight into disease mechanisms.

Introduction

The vacuolar H^+-ATPase (V-ATPase) is a highly conserved enzymatic complex that functions in an ATP-dependent manner to pump protons across membranes and acidify organelles. The V-ATPase is comprised of a peripheral V_1 domain and an integral V_0 domain (**Fig. 1**). The V_1 domain is responsible for the hydrolysis of ATP creating the necessary energy to translocate protons through the V_0 domain via a rotational mechanism.[1] The V-ATPase plays a crucial role in many cellular processes involving membrane trafficking by creating a proton/pH gradient used by several different types of transporters.[1,2]

The human V-ATPase, comprised of 13 different subunits, is encoded by 23 genes (**Supplementary Table 1**). This genetic redundancy allows for the formation of tissue-specific V-ATPase complexes, including in synaptic vesicles (SVs) where it creates the necessary proton/pH gradient to load various neurotransmitters.[1,2] To date, twelve genes corresponding to eight different subunits of the V-ATPase have been associated with human disease (**Supplementary Table 1**).[3-13] Early-onset epilepsy has been observed in patients with variants in either *ATP6V1A* or *ATP6V0A1*, with heterozygous, *de novo* variants leading to less severe presentations when compared to patients with biallelic variants.[14-16] Pathogenic variants in *ATP6V1B2* can cause epileptic conditions such as Zimmerman-Laband (MIM#616455) and DOORS syndromes, or deafness and nail dysplasia without epilepsy (DDOD, MIM#124480).[11,12,17,18] An accessory protein to the V-ATPase, encoded by *ATP6AP2*, is associated with X-linked syndromic intellectual disability that can present with or without epilepsy (MIM#300423).[19,20]

ATP6V0C, a three-exon gene (**Fig. 2A**) located on human chromosome 16p13.3, encodes the 155 amino acid c-subunit of the V_0 domain which along with the c″ subunit (encoded by *ATP6V0B*) forms the intramembrane c-ring that facilitates the movement of protons across the membrane (**Fig. 1**).[21] The process of proton translocation is reliant on a glutamate residue at position 139 (p.E139) in ATP6V0C as well as an arginine residue (p.R735) in ATP6V0A.[1]

We previously described patients with developmental delay, intellectual disability, microcephaly, and seizures with 16p13.3 microdeletions encompassing a minimal overlapping region that included *TBC1D24*, *ATP6V0C*, and *PDPK1*.[22] By reviewing the known function(s) and expression patterns of genes in the minimal overlapping region, we proposed haploinsufficiency of *ATP6V0C* as the primary contributor to the clinical features of

16p13.3 microdeletion syndrome.[23] However, we did not provide any functional evidence to support our claim.

Most recently, Ittiwut *et al.*[24] reported a *de novo* stop-loss variant in *ATP6V0C* in an individual with epilepsy and intellectual disability. Analysis of RNA derived from the patient's leukocytes revealed that, as expected, the mutant transcript escaped nonsense mediated decay (NMD). The authors proposed haploinsufficiency as the likely pathomechanism given the observed decrease in mRNA levels; however, a dominant negative effect is also possible given the transcript escape from NMD. Hence, thus far it is unknown if *ATP6V0C* missense variants are a cause of human disease, and the mechanistic basis of *ATP6V0C*-associated human disease is unclear.

In this study, we report the identification of heterozygous *ATP6V0C* missense variants in 27 patients with a novel syndrome of developmental delay, epilepsy, and intellectual disability. We present multiple lines of computational and functional analyses to demonstrate that these variants are pathogenic and disrupt V-ATPase activity.

Materials and methods

Identification of Individuals with *ATP6V0C* Variants

Authorization was obtained at each site to release deidentified patient medical information to study investigators and when applicable informed consent was obtained through protocols approved by the institutional review boards at each site of patient recruitment. Patients with *ATP6V0C* variants were identified via GeneMatcher, and by interrogating the 100,000 Genomes database, the Deciphering Developmental Disorders (DDD) study, and ClinVar.[25-27] We also screened whole-exome sequencing (WES) data from epilepsy patients referred for genetic testing at EGL Genetics. Three patients (Patients 2, 13 and 27) were previously reported in other publications.[24,25,28] For Patients 2 and 27, clinical information was obtained from the previous publications, whereas the referring clinician provided clinical information for Patient 13. Patient 5 was reported in ClinVar and clinical information was provided by the depositing organization (**Supplementary Table 2**). Clinical information for all other patients was collected using a custom form provided to each site.

Sequencing and Analysis of Sequence Data

Whole-exome or whole-genome sequencing was performed on patient DNA extracted through standard protocols. All libraries were sequenced on Illumina HiSeq systems.

Sequence alignment and variant calling were performed at each site and further details are provided in **Supplementary Table 2**. When possible, *ATP6V0C* variant segregation was confirmed with Sanger sequencing using standard protocols.

Lollipop and Missense Tolerance Ratio Diagram

The Lollipop diagram was created as previously described using the UniProt accession number, P27449.[29,30] Non-synonymous and synonymous population variants were downloaded from gnomAD (v.2.1.1).[31] Resulting diagrams of gnomAD and patient variants were merged into a single image for ease of visualization, and the locations of the transmembrane domains were superimposed over the resulting image. A missense tolerance ratio (MTR) plot was generated using MTR-Viewer v2, with a codon window size of 21, on the ENST00000330398 transcript.[32]

Drosophila Studies

The Drosophila ortholog, Dmel\Vha16-3 (CG32090), was knocked-down using pan-neuronal (elaV-GAL4) expression of a gene-specific RNAi construct (VDRC-102067), provided by the Vienna Drosophila Resource Center. As a control, an RNAi to GFP was used. Seizure-like behavior was elicited using electroshock of wall-climbing third instar larvae as described in Marley and Baines 2011.[33] Drugs, solubilized in DMSO, were fed to larvae by mixing (at 2mM) in molten fly food which was then allowed to cool and set before being seeded with first instar larvae.

In silico Variant Modeling

Patient and gnomAD variants were displayed in the context of a structure for the V_0 domain of human V-ATPase (PDB: 6wlw).[21,34] PyMOL and Swiss PDB Viewer were used for visualization of protein structure.[35]

Saccharomyces cerevisiae Strains and Plasmids

E. coli and yeast manipulations were performed following standard molecular biology protocols.[36] The *vma3::kanMX* yeast strain (*vma3Δ,* Cat No. YSC6273-201929081) was obtained from GE Dharmacon and is isogenic with BY4741 (*MATa his3Δ leu2Δ met15Δ ura3Δ*). Plasmids are listed in **Supplementary Table 3**. A plasmid (pKM16) containing the promoter and wild-type open reading frame for *VMA3* (the yeast ortholog of *ATP6V0C*) was generated by amplifying a 924bp fragment from *S. cerevisiae* gDNA and cloning it into pRS316 using *BamHI* and *SacI* (Forward cloning primer: 5' taagcaggatccagcaatgaaataggccgtctac, Reverse cloning primer: 5'

taagcagagctccttgaaatgaggtagtttgg) .[37] pKM16 was used as the backbone to generate all variants via conventional cloning techniques or the QuikChange XL Site-Directed Mutagenesis Kit (Agilent Technologies). Sanger sequencing was performed to confirm the presence of each variant as well as the absence of unwanted substitutions.

Plasmids were transformed into the *vma3Δ* strain and selected on plates containing synthetic minimal media plus dextrose supplemented to select for a *URA3* plasmid (SD-ura). Selected transformants were maintained on SD-ura throughout the course of experiments.

Serial Dilution Spotting Assay

Liquid cultures of transformants were grown at 30°C overnight in SD-ura adjusted to a pH of 5.5. 1 OD_{600} per ml of cells was collect and suspended in dH_20. Serial 10-fold dilutions were spotted onto SD-ura plates. Plates were imaged after incubation at 30°C for 48 hours.

LysoSensor Uptake and Confocal Imaging

Cells were collected at OD_{600} 0.6-1.0 and incubated with LysoSensor Green DND-189 (Invitrogen, Cat# L7535) as previously described.[38] Cells were resuspended in 1X PBS (pH 7.6) to an OD_{600} of 0.6, deposited on 1.5% agarose pads, and visualized immediately. Images were taken at room temperature using a confocal laser scanning microscope (A1R HD25, Nikon) with an Apo TIRF 60x 1.49 NA oil immersion lens, WD 0.12mm (Nikon). Images were acquired using NIS-Elements (AR 5.21.02, Nikon) and processed using FIJI. All cells visible in the DIC channel were selected, the selection was copied to the FITC channel, and the mean grey area was calculated for each cell. Measurements were corrected for background signal by subtracting the mean grey area of a background only selection from each image. Two biological replicates, in separate experiments, totaling 71-132 cells for each variant were analyzed.

Generation of Growth Curves

Liquid cultures of transformants were grown at 30°C overnight in SD-ura adjusted to a pH of 5.5. Overnight cultures were diluted 1:20 in dH_20 and further diluted 1:10 in YPD, pH 5.5, with 5mM, 100mM or 200mM $CaCl_2$. OD_{600} measurements were taken every 15 minutes for 30 hours at 30°C with shaking using an ELx808 plate reader (BioTek). Three independent transformants were assayed in triplicate for each variant. The R package, GrowthCurver, was used to calculate the empirical area under the curve (eAUC) for each replicate.[39]

Caenorhabditis elegans Studies

All *C. elegans* strains were cultured and handled as per standard methods. All experiments were carried out at 20°C. Mutations were knocked-in via CRISPR/Cas9, and homozygous worms were studied. Strains used in this project are described in **Supplementary Table 4**.

Paralysis Assays

In three separate experiments, 30-40 L4 worms (in triplicate) were picked to standard NGM plates either with 51mM NaCl (physiological conditions), or with 200mM or 300mM NaCl, and scored daily for paralysis starting the day after they were picked. A total of 270-360 worms were tested per condition. Worms were counted as paralyzed if they failed to move their body upon prodding with a platinum wire and were considered dead if they failed to move their head and showed no pharyngeal pumping when prodded. Dead or lost animals were censored from statistical analyses. Worms were transferred every 2 days to avoid progeny.

Lifespan Assays

Lifespan experiments were conducted similarly to paralysis assays. Two separate experiments were performed using 35-40 worms in triplicate, leading to a total 315-360 worms tested per condition. Worms were counted every second day from day 1 of adulthood until death. Lost animals were censored from statistical analyses, paralyzed worms were not censored and were kept until death.

Liquid Culture Motility Assays

Synchronized day 1 adult worms were transferred into 200uL of M9 buffer with or without 350mM NaCl in each well of a 96 well plate, to a density of 30 worms per well. Motility was automatically analyzed for 4 hours using a WMicrotracker-One plate reader (PhylumTech).

WormLab Analysis

Synchronized day 1 adult worms were video recorded for 30-33 seconds using a Leica Stereomicroscope S9i. Automated movement and worm size analyses were conducted using WormLab software (MBF Biosciences) which tracks individual worms from the recorded videos. Activity index is defined by the brush stroke (area "painted" by the animal's body in a single complete stroke) normalized by the time taken to perform two strokes. Wave initiation rate is defined as the number of body waves initiated from either the head or the tail per minute. Swimming speed was measured over a two-stroke interval.[40] For body size analysis, worms were recorded on bacteria free NGM plates. For swimming parameters, worms were

placed in M9 with 500mM NaCl and recorded 30 minutes later. At least 50 worms were recorded in two independent experiments.

Aldicarb Sensitivity Assays

Worms were grown on standard NGM plates until day 1 of adulthood and then transferred to NGM plates containing 1mM aldicarb. Paralysis was assayed every 30 minutes for 2 hours. Animals were counted as paralyzed if they failed to move upon prodding with a platinum wire.

Statistical Analyses

Drosophila recovery time was analyzed using one-way ANOVA with Dunnett's post-hoc test for multiple comparisons. Recovery time after drug treatment was normalized to the vehicle only control. A Fisher's Exact test was used to demonstrate the presence of a variant hot-spot in the fourth transmembrane domain of ATP6V0C. For LysoSensor, fluorescence values for each cell measured were normalized to the mean fluorescence of the wild-type rescue. For the growth rate assay, eAUC values were normalized to the mean eAUC of the wild-type rescue within each plate. A one-sample t-test was used to compare the mean fluorescence and eAUC for each variant to a hypothetical mean of 100 (representing the wild-type rescue). Significance levels were corrected for multiple comparisons using a Bonferroni correction (LysoSensor and growth at 5mM, $\alpha = 0.0003125$; 100mM, $\alpha = 0.00714$; 200mM, $\alpha = 0.00833$). A two sample t-test (two-tailed) was used to compared p.G103S to p.F137L at 200mM. Paralysis curves and lifespan assays were compared using the log-rank (Mantel–Cox) test. The liquid culture motility assays (WormTracker) results were analyzed using two-way ANOVA to compare each variant to the wild-type N2 strain. WormLab results were analyzed using a one-way ANOVA with a Dunnett's post-hoc test for multiple comparisons to compare each variant to the wild-type N2 strain. The WormLab data is presented as box and whisker plots indicating minimal and maximal data points. Normalization and statistical analyses were carried out using Prism 9.0 (GraphPad Software Inc.). All data is presented as mean ± SEM and $\alpha = 0.05$ was used unless otherwise noted.

Data and Reagent Availability

All strains and plasmids (**Supplementary Tables 3 and 4)** used in this study are available upon request. The human datasets presented in this article are not publicly available due to ethical and privacy restrictions. Requests to access the human datasets should be directed to the corresponding authors.

Results

Identification of *ATP6V0C* Variants in Patients

We identified 27 patients with heterozygous *ATP6V0C* variants through GeneMatcher, 100,000 Genomes database, the DDD study, ClinVar, published literature, and EGL Genetics. Of the 27 patients, 22 had missense substitutions (18 variants were unique), 4 had frameshifting variants, and 1 had a stop-loss variant (**Table 1**). The variants p.A138P, p.A149T, and p.L150F were recurrent, each being seen in two or more unrelated individuals. Different substitutions at p.A95 and p.L150 were also observed. Patients 4, 9, 15 and 19 were each found to be mosaic for their identified *ATP6V0C* variant.

Multiple lines of evidence support the pathogenicity of the identified patient variants. Firstly, all patient variants were absent from the Genome Aggregation Database (gnomAD, v.2.1.1), which is compilation of exome and genome sequencing data from large-scale sequencing projects for which efforts have been made to remove individuals affected by severe pediatric disease. Secondly, in 24 patients where biologic parent DNA was available, the variants were found to have occurred *de novo*. Thirdly, all missense substitutions affected highly conserved residues (**Fig. 2B**), with 17 out of the 18 unique missense variants having CADD scores that placed them in the top 1% of predicted deleterious variants. Lastly, *ATP6V0C* has a predicted intolerance to missense and loss of function variation with only 21 population missense variants observed in gnomAD compared to the expectation of 108 (observed/expected = 0.19) and 0 loss of function variants observed compared to the expectation of 4.5 (**Fig. 2C-D)**. In addition, all *ATP6V0C* gnomAD variants are observed at low frequencies (three times or less).[41] Taken together, when the ACMG/AMP variant classification guidelines are applied, all *ATP6V0C* variants identified in the patients are predicted to be likely pathogenic or pathogenic (**Supplementary Table 2**).[42]

ATP6V0C Variants Cause a Human Syndrome of Developmental Delay, Epilepsy, and Intellectual Disability

The primary clinical presentation of the identified patients was developmental delay with early-onset epilepsy and intellectual disability **(Table 1**). The mean age of seizure onset was 24.6 ± 8.0 months, with 14 of 18 patients for whom this information was available having onset prior to 24 months. Based on clinical information from 19 patients, the most common seizure types observed were generalized tonic-clonic (12/19), focal (7/19), atonic (6/19), and myoclonic (5/19). Intellectual disability, ranging from mild to severe, was seen in 16/16

patients who were old enough for a formal diagnosis and for whom this information was available. Development delay was seen in 21/23 patients. Twenty-one patients had MRIs with thirteen showing abnormalities (**Supplementary Table 2**). Common findings in MRIs included agenesis/hypoplasia of the corpus callosum (**Supplementary Fig. 2**) or cerebellar vermis (Patients 5, 6, 18, 20 and 26), and delayed myelination (Patients 6, 18, 22 and 24). Four patients were reported to have cardiac abnormalities: Patient 3 had pulmonary valve stenosis, Patient 6 had a thickened left ventricular wall, Patient 7 had a heart murmur, and Patient 13 exhibited several cardiac defects including hypertrophic cardiomyopathy, mitral valve prolapse, and mild to moderate mitral valve regurgitation. Patients 5 and 24 showed dental enamel defects, with Patient 24 lacking dental enamel. It should be noted that Patient 7 also has a *de novo* 2.3Mb deletion in 20q11.22-11.23 which has been associated with developmental delay and dysmorphism, and Patient 13 has biallelic variants in *LZTR1* which has been associated with Noonan-like syndrome (MIM#605375).[43]

Collectively, these data show that *ATP6V0C* variants cause a human syndrome of developmental delay, intellectual disability, and epilepsy. Furthermore, as most individuals were ascertained on the basis of genotype (i.e., having a variant in *ATP6V0C*), their phenotypic convergence on reverse phenotyping further supports the pathogenicity of the variants described in this study.[44]

ATP6V0C Knockdown in Drosophila Results in Seizure-like Behavior

Based on our hypothesis that haploinsufficiency of *ATP6V0C* drives the neurological phenotype of 16p13.3 microdeletion syndrome and the identification of patients with frameshift variants, we first tested the consequences of ATP6V0C knockdown in Drosophila.[23] The orthologous protein in Drosophila, Dmel\Vha16-3, (CG32090), shows 78% amino acid identity to ATP6V0C. CG32090 was knocked-down via pan-neuronal expression of a gene-specific RNAi construct (VDRC-102067). The same pan-neuronal driver line (elaV-GAL4) driving expression of GFP RNAi (elaV>GFP RNAi), and the homozygous 102067 RNAi line without the elaV-GAL4 driver (102067 RNAi) were used as controls. Following knock-down of CG32090 (elaV>102067 RNAi), wall climbing third instar larvae showed a significant increase in recovery time (i.e., longer seizure-like behavior) after electroshock ($p < 0.0001$, one-way ANOVA, **Fig. 3A**). Pre-treatment of these larvae with a variety of established antiepileptic drugs resulted in significant reductions in recovery time with levetiracetam and topiramate ($p < 0.001$), and to a lesser extent with lamotrigine

and valproate (p < 0.01 and < 0.05, respectively, **Fig. 3B**). Phenytoin, at the same concentration (2mM in fly food) did not significantly alter recovery time. These results are consistent with the hypothesis that haploinsufficiency of *ATP6V0C* contributes to seizures.

ATP6V0C Variants Are Predicted to Interfere with V-ATPase Rotary Mechanism

Higher conservation across ATP6V0C orthologs was seen at sites of patient variants compared to gnomAD variants (**Supplementary Fig. 1**). To understand the basis of pathogenicity of the *ATP6V0C* patient missense variants, we first turned to *in silico* modelling. Upon hydrolysis of ATP, the c-ring (comprised of nine copies of ATP6V0C and one copy of ATP6V0B) rotates within the membrane delivering protons to the ATP6V0A subunit (encoded by *ATP6V0A*) for transport across the membrane (**Fig. 1**).[21] Transmembrane (TM) domains 2 and 4 of ATP6V0C are outward facing and interact with ATP6V0A during this rotational mechanism.[45,46] The location of patient variants shows an enrichment within TM domains and the presence of a 'hot-spot' in the fourth TM of ATP6V0C (p = 0.006, Fisher's Exact test, **Fig. 2C**). When viewed structurally, some patient and gnomAD variants are located at sites of packing between c-ring subunits; however, many more patient variants are located outward-facing from the c-ring so as to potentially interfere with interactions between mutant ATP6V0C subunits and the ATP6V0A subunit (**Fig. 4A-B**). These data raise the possibility that outward facing *ATP6V0C* missense variants may have a dominant negative effect.

ATP6V0C Patient Variants Are Deleterious in Yeast

Budding yeast, *S. cerevisiae*, possesses an *ATP6V0C* ortholog, *VMA3*, which shares 72% amino acid identity and a conserved four transmembrane protein structure. *S. cerevisiae* has been previously used to study the functional effects of variants in other V-ATPase subunits.[8,47-50] Given that all identified patient missense variants affected residues that are conserved between human and yeast, we expressed 12 of the patient variants in *VMA3* using a centromeric plasmid in a *vma3Δ* yeast strain (**Supplementary Fig. 1, Supplementary Table 3**). Six additional variants were identified after completion of these experiments and, therefore, were not modeled in yeast.

We also examined the functional effects of three population variants in *ATP6V0C* from gnomAD (p.R48W, p.G103S, p.M131I; **Supplementary Fig. 1, Supplementary Table 5**) on V-ATPase function. p.R48W was chosen as it effects the same residue as the p.R48P patient variant. p.G103S and p.M131I were chosen as they have the highest CADD scores for

variants seen twice and once, respectively, in gnomAD. The altered residues are also conserved between human and yeast (**Supplementary Fig. 1**). All *ATP6V0C* variants in gnomAD (21 total) are rare (**Supplementary Fig. 1**), being seen no more than three times out of approximately 250,000 alleles. In addition, we also generated and tested p.E139A, which removes the glutamate residue necessary for V-ATPase function.[1]

To first establish the ability of the *vma3Δ* strain to grow when transformed with plasmids containing patient or population variants, a serial dilution spot assay was performed on SD-ura plates. We confirmed the ability of all transformants to grow under no selective V-ATPase pressure, thereby allowing us to examine V-ATPase function in our yeast model (**Supplementary Fig. 3**).

LysoSensor Green DND-189 ($pK_a \sim 5.2$) is an acidotropic dye that accumulates in the membranes of vacuoles. Upon protonation, quenching of the fluorescent probe is relieved and fluorescent intensity increases in a pH dependent manner. It has been previously demonstrated that V-ATPase activity in yeast and fluorescent intensity of LysoSensor Green are correlated.[38] We looked for rescue of V-ATPase function by transformation of each patient or population variant into the *vma3Δ* strain. Nine patient variants and p.E139A resulted in little to no fluorescence (**Fig. 5A, Supplementary Fig. 4**). Two patient variants (p.G63A and p.L150F) and two gnomAD variants (p.R48W and p.G103S) showed intermediate levels of fluorescence intensity compared to the wild-type rescue. One gnomAD variant (p.M131I) and one patient variant (p.F137L) show levels of fluorescence intensity that were comparable to wild-type rescue. Overall, 11 of 12 patient variants and all gnomAD variants elicited significant decreases in fluorescence intensity when compared to the wild-type rescue ($p < 0.01$, one sample t-test, **Fig. 5A**).

V-ATPase, and therefore ATP6V0C, function is required for yeast to grow at increased $CaCl_2$ concentrations.[47,51] To further examine the consequences of patient *ATP6V0C* variants on V-ATPase function, transformants were used to inoculate YPD with 5mM $CaCl_2$ and growth curves were generated for each variant (**Fig. 5B-E**). Eight patient variants and p.E139A showed negligible growth at 5mM $CaCl_2$. The remaining four patient variants and all gnomAD variants showed varying degrees of growth at 5mM $CaCl_2$. Overall, significantly less growth compared to wild-type rescue was seen for 11 of 12 patient and the three gnomAD variants tested ($p < 0.0001$, one sample t-test, **Fig. 5F**). The results seen at 5mM $CaCl_2$ mirrored those seen with LysoSensor uptake ($r^2 = 0.7921$, **Supplementary Fig. 5**).

Next, patient variants that grew at 5mM $CaCl_2$ along with the three gnomAD variants were tested at 100mM and 200mM $CaCl_2$ to determine whether a higher concentration of calcium would provide further separation of variants relative to the wild-type rescue. At 100mM $CaCl_2$, p.L150F showed almost no growth compared to wild type ($p < 0.0001$, one sample t-test, **Supplementary Fig. 6A-B**) while the three other patient variants (p.G63A, p.V74F, p.F137L) showed intermediate growth relative to the wild-type rescue. The growth of one gnomAD variant (p.M131I) was similar to the wild-type rescue, while p.R48W and p.G103S both showed less growth relative to the wild-type rescue. The three patient variants with intermediate growth at 100mM $CaCl_2$ and the three gnomAD variants were then tested at 200mM $CaCl_2$ (**Supplementary Fig. 6C-D**). Significantly less growth was seen with the three patient variants compared to the wild-type rescue ($p < 0.0001$), while two gnomAD variants (p.R48W and p.M131I) were comparable to the wild-type rescue. p.G103S showed less growth relative to the other gnomAD variants (p.R48W and p.M131I), but still yielded a significantly larger eAUC (**Supplementary Fig. 6D**) compared to the best growing patient variant at 200mM $CaCl_2$, p.F137L (59.22 ± 2.278 vs. 45.63 ± 2.243, $p = 0.0006$, two sample t-test).

Assessment of Three Patient Variants in *C. elegans*

Next, we assessed the effects of a subset of patient *ATP6V0C* variants on neurological function using *C. elegans.* Worms express three orthologous genes to *ATP6V0C* in neurons, *vha-1, vha-2,* and *vha-3*. VHA-2 and VHA-3 have identical amino acid sequences and share 66.7% amino acid identify with ATP6V0C, while VHA-1 has slightly less homology to ATP6V0C at 63% amino acid identity. The variants that were selected for further analysis were distributed throughout the protein, showed tolerance to 5mM $CaCl_2$ in the yeast growth assay, and were identified in patients with severe neurocognitive deficits and poly-medicated epilepsy. Specifically, we studied p.F137L (corresponding to p.F143L in VHA-2) and p.G63A and p.L150F (corresponding to p.G69A and p.L156F, respectively, in VHA-3*)*. A fourth strain carrying the p.A95T variant (corresponding to p.A101T in VHA-2) was generated but caused sterility in homozygous worms and was not studied further.

Worms expressing each variant were shorter and smaller than N2 (wild-type) controls at day 1 of adulthood, indicating a morphological delay even in ideal physiological conditions ($p < 0.05$, one-way ANOVA, **Fig. 6A-B**). When tested in liquid physiological M9 over a 4-hour period, movement of day 1 young adult worms with each mutation was comparable to N2 worms (**Fig. 6C**)**.** However, when motor function was examined under osmotic stress

conditions (350mM NaCl), mutants expressing p.G63A and p.F137L exhibited significantly reduced movement scores when compared to N2 worms ($p < 0.01$, two-way ANOVA, **Fig. 6D**). Although mutants expressing p.L150F also exhibited less movement than N2 worms, this difference was not statistically significant ($p = 0.0869$).

We next compared paralysis and lifespan of each mutant strain with N2 worms when maintained on NGM plates under physiological conditions or exposure to osmotic stress (200mM and 300mM NaCl). All mutants showed greater levels of paralysis when compared to N2 worms over a 14-day period, and these differences were strongly exacerbated in the presence of osmotic stress ($p < 0.0001$, log-rank (Mantel–Cox) test, **Fig. 6E-G**). Lifespans of the mutant strains were also reduced when compared to N2 worms when maintained under physiological conditions and osmotic stress ($p < 0.0001$, log-rank (Mantel–Cox) test, **Fig. 6H-J**).

To compare fine motor phenotypes, we exposed the mutant strains and N2 worms to liquid M9 with 500mM NaCl for 30 minutes and analyzed movement using WormLab. Activity index and wave initiation were significantly increased in the mutant strains when compared to N2 worms ($p < 0.05$), but swimming speeds were not significantly altered, suggesting increased but uncoordinated movements ($p > 0.05$, one-way ANOVA, **Fig. 7A-C**).

To test if the mutant strains have an impairment in nervous system signaling, we added an acetylcholinesterase inhibitor, aldicarb, to NGM plates and scored the number of paralyzed worms over a 2-hour period. Aldicarb causes an accumulation of acetylcholine in neuromuscular junctions resulting in muscle hypercontraction and acute paralysis, and can be used to evaluate if there is dysfunction of either GABA or acetylcholine signalling.[52,53] To confirm proper aldicarb effect, we included unc-47(e307) and unc-64(e246) mutants. Unc-47(e307) mutants are hypersensitive to aldicarb due to the lack of a vesicular GABA transporter gene (orthologous to *SLC32A1* in humans) required for GABA transmission.[54] Unc-64(e246) (orthologous to *STX1A* in humans) mutants have reduced cholinergic neurotransmission, making them resistant to aldicarb-induced paralysis.[55,56] Worms expressing each patient variant showed greater paralysis in presence of aldicarb, compared to N2 worms ($p < 0.0001$, log-rank (Mantel–Cox) test, **Fig. 7D**).

Discussion

In this study, we report the identification of heterozygous *ATP6V0C* variants in 27 patients with neurodevelopmental phenotypes. In general, this cohort of patients presented with

development delay, early-onset epilepsy (mean age of onset: 24.6 ± 8.0 months), and varying severities of intellectual disability. Five patients with MRIs show hypoplasia or agenesis of the corpus callosum. Congenital cardiac abnormalities were also observed in four patients. Interestingly, congenital heart defects have been reported in patients with pathogenic variants in *ATP6V1A* and *ATP6V1E1*.[3]

ATP6V0C is an evolutionary constrained gene as reflected by the high degree of amino acid homology between the human and yeast orthologs (72%), human and worm orthologs (63-67%), and human and Drosophila orthologs (78%), and the low number of missense variants in gnomAD (n=21 compared to an expected 108.5).[31] Of the 18 unique patient missense variants, 16 are located in TM domains, with nine in TM4 which encompasses the p.E139 residue that is required for proton transport by the V-ATPase.[1] Consistent with evolutionary constraints on TM4, only one variant in gnomAD is located in this region of the protein (**Fig. 2C**).

Interestingly, four patients (Patients 4, 9, 15 and 19) were found to be mosaic for their identified *ATP6V0C* variant. Based on the available clinical information, the seizure phenotype of these patients may be less severe than for those with a germline variant (**Table 1**). Patient 4 (p.M53R) has seizure-like episodes that started at 14 months, but are not supported electrographically, Patient 15 (p.I132N) had seizure onset at 12 years of age, and Patient 19 (p.G142D) has not reported any seizure or seizure-like episodes. In contrast to the other mosaic patients, Patient 9 (p.A95T) had seizure onset at 10 months. p.A95T also resulted in decreased V-ATPase activity in yeast (**Fig. 5**) and sterility in homozygous worms (**Supplemental Table 4**). The timing of the post-zygotic mutation event, and the affected tissues, can have a large influence on phenotypic presentation and severity in patients with somatic mosaicism, underlying differences in clinical presentation between patients with germline and mosaic variants.[57] Previous work has demonstrated the utility of identifying somatic mosaicism for clinical and genetic counseling outcomes in patients.[58]

Nine copies of ATP6V0C and one copy of ATP6V0B assemble to form the intramembrane c-ring of the V-ATPase which uses a rotary mechanism to translocate protons across the membrane (**Fig. 1**).[21] Normally, frameshifting variants are predicted to cause NMD of the mutant mRNA, which would result in reduced protein levels. However, two of the four frameshift variants (c.340_355del16 and c.352_362delins) are located in last exon of *ATP6V0C* and are thus expected to escape NMD. The two frameshift variants in exon 2 may also escape NMD given the proximity of c.134_135delCT to the start codon and c.214delG being within 50bp of the last exon-exon junction (**Fig. 2A**).[59] Additionally, modeling showed

that outward facing missense variants might act as a 'stone in the gear' between ATP6V0C and ATP6V0A inhibiting the rotatory mechanism, consistent with a dominant negative effect and the mechanism of action of V-ATPase inhibitors such as bafilomycin and archazolid **(Fig. 4A-B)**.[45,60] Therefore, we speculate that missense variants and those predicted to escape NMD act via a dominant negative mechanism, while nonsense variants and microdeletions containing *ATP6V0C* act via haploinsufficiency as demonstrated by our Drosophila data (**Fig. 3**). However, additional studies, including the quantification of mRNA levels associated with each variant, are needed to delineate disease mechanisms more clearly.

Twelve disease-associated missense variants were examined in yeast. When the uptake of LysoSensor was measured, we saw that nine variants were associated with little to no fluorescence, indicating significant reduction or loss of V-ATPase activity. Higher levels of fluorescence were seen when the p.G63A, p.F137L, and p.L150F patient variants were expressed (**Fig. 5A, Supplementary Fig. 4**). Growth curves generated by yeast expressing the 12 patient variants mirrored observations from the LysoSensor assay (**Supplementary Fig. 5)**, with most variants resulting in little or no growth, and intermediate levels of growth observed with the p.G63A, p.V74F, p.F137L, and p.L150F variants (**Fig. 5F**). To further examine the effect of these intermediate variants on developmental and neurological function, we modeled p.G63A, p.F137L, and p.L150F in worms. Expression of all three variants resulted in morphological delay as indicated by reduced body size and length at day 1 of adulthood (**Fig. 6A-B**). Mutant worms also exhibited greater levels of paralysis and decreased lifespan when compared to N2 worms, and these phenotypes were exacerbated under osmotic stress (**Fig. 6E-J**). Mutants also exhibited increased activity and wave initiation rates, but speed was unaltered, suggestive of hyperactive and uncoordinated movement (**Fig. 7A-C**). The p.A95T variant which showed almost no V-ATPase function when tested in yeast (**Fig. 5**), resulted in homozygous sterility in worms, suggestive of a greater impact on V-ATPase function.

Additionally, we functionally examined, in yeast, three variants from gnomAD (p.R48W, p.G103S, p.M131I) that had high CADD scores and were predicted to be damaging by SIFT or Poly-Phen2 which contrasts the assumption that population variants would be benign (**Supplementary Table 5**). Expression of p.R48W and p.M131I resulted in growth that was more similar to the wild-type rescue compared to patient variants at 5mM $CaCl_2$ and did not significantly differ from wild-type rescue as higher concentrations of $CaCl_2$ were tested (**Fig. 5F, Supplementary Fig. 6**). p.G103S, which had the highest CADD score of the gnomAD variants tested, resulted in significantly decreased growth compared to the wild-

type rescue across all $CaCl_2$ concentrations tested (**Fig. 5F, Supplementary Fig. 6**). Nevertheless, p.G103S still yielded a significantly larger eAUC when compared to the best growing patient variant (p.F137L), suggesting the possibility of a level of decrease in V-ATPase activity that can be tolerated. However, we cannot exclude the possibility that mild clinical features could be associated with p.G103S or other rare gnomAD variants. Additional testing of population variants could establish the minimum level of V-ATPase activity required to maintain normal function. Such information would also aid in variant classification when novel patient variants are identified in the future.

The cellular mechanisms that explain the clinical features in patients with pathogenic variants in *ATP6V0C* are not yet known. However, given the importance of acidification driven by the V-ATPase in many cellular processes, it is likely that several pathways are impacted. Firstly, the acidification of SVs within the central nervous system by the V-ATPase allows transporters, such as VGLUTs and VGAT, to load their respective cargo.[61,62] Our modeling data predicts that outward facing patient variants would interfere with the interaction between ATP6V0C and ATP6V0A (**Figure 4**). Interestingly, patients with pathogenic *ATP6V0A1* variants (encoding ATP6V0A) present with developmental delay, epilepsy, intellectual disability and cerebellar atrophy, similar to patients with pathogenic *ATP6V0C* variants.[15] Recent work has shown that primary cortical neurons from *Atp6v0a1*$^{A512P/A512P}$ mice, modeling a variant identified in a patient, have decreased SV neurotransmitter content and form fewer synapses.[15] Given the functional interaction between ATP6V0C and ATP6V0A1, we speculate that synaptic defects likely contribute to disease pathology in patients with pathogenic *ATP6V0C* variants. These defects may also be independent of the ATPase activity of the V_1 domain as the V_0 domain is involved in neurotransmitter release independent of its acidification of SVs.[63-65]

The V-ATPase also plays an important role within the trans-Golgi network (TGN) and inhibition of V-ATPase driven acidification can lead to improper trafficking and sorting of various membrane bound proteins, including neuropeptides and neuropeptide receptors.[66-68] Additionally, pathogenic variants in *SLC9A7* in patients with developmental delay, intellectual disability, and muscle weakness have been shown to cause alkalization of the TGN.[69] Therefore V-ATPase dysfunction may also lead to altered synaptic signaling via disruption of trafficking and sorting of receptors to the synapse. Consistent with this prediction of altered synaptic signaling, worms expressing the p.G63A, p.F137L, and p.L150F variants displayed greater sensitivity to aldicarb and higher rates of paralysis compared to N2 worms (**Fig. 7D**).

Lastly, perturbations of lysosomal and autophagy pathways may also contribute to the epilepsy and neurodevelopmental phenotypes seen in these patients. The V-ATPase plays an essential role in acidifying endosomes, lysosomes, and autophagosomes which ultimately creates the environment needed for proper trafficking and maturation of endocytic organelles and acid hydrolase function within the autophagy pathway.[2,70] Previous work by Nakamura *et al.*[71] demonstrated that the V-ATPase is required for protein degradation from autophagic bodies in yeast vacuoles and Fassio *et al.*[14] showed impairments in autophagic flux caused by pathogenic variants in *ATP6V1A*. In recent years, the contribution of impaired autophagy to neurodegenerative and neurodevelopmental disorders, including epilepsy, has risen in importance.[14,72,73] We hypothesize that the epilepsy and other neurodevelopmental phenotypes seen in patients with pathogenic V-ATPase variants may be due to a combinatorial effect of impaired synaptic signaling, trafficking and sorting of various membrane bound proteins, and defects along the endomembrane system including the lysosomal/autophagy degradation pathway. Further functional studies will be required to more thoroughly understand the mechanisms by which *ATP6V0C* variants lead to disease.

The prevalence of neurodevelopmental disorders, including epilepsy, resulting from variants in *ATP6V0C* is likely underestimated as this gene, to the best of our knowledge, is not currently included on commercially available epilepsy or intellectual disability gene panels. Of the 23 genes that encode for a subunit of the V-ATPase, twelve, including *ATP6V0C*, are associated with disease. Ten additional members of the complex are expressed in the central nervous system but are currently not associated with disease (**Supplemental Table 1**).[74] Screening of these genes for potential pathogenic variants in patients with disorders such as epilepsy and intellectual disability should be undertaken. Additionally, longitudinal studies in patients with *ATP6V0C* mutations, and the identification of additional patients, will play an important role in resolving the full spectrum of co-morbidities associated with altered ATP6V0C and V-ATPase function.

In summary, we report 27 patients with heterozygous *ATP6V0C* variants who presented with developmental delay, early-onset epilepsy, and intellectual disability. *In silico* modeling suggests that the majority of patient missense variants disrupt the interaction between the ATP6V0C and ATP6V0A subunits, and functional testing revealed that these variants decrease V-ATPase activity in yeast, and impair motor function, growth, and lifespan in worms. Further work is needed to fully elucidate the mechanism(s) by which altered *ATP6V0C* function lead to the range of observed clinical phenotypes, and whether

other V-ATPase subunits not currently known to cause disease harbor pathogenic variants in patients with neurodevelopmental disorders without a current genetic diagnosis.

Acknowledgements

We would like to thank the patients and their families for their participation in this study. We would also like to thank Dr. Victor Faundez, Dr. Anita Corbett, Dr. Sara Leung, and Dr. Meleah Hickman (Emory University) for helpful advice and for providing reagents and equipment. Figure 1 was adapted from "V-ATP synthase", by BioRender.com (2022); retrieved from https://app.biorender.com/biorender-templates.

Funding

This study was supported by a training grant appointment to K.A.M (5T32GM008490), and an Emory University Research Council grant to A.E. J.B. is funded by a senior clinical investigator fellowship of the FWO-Flanders. This study was also supported in part by the Emory University Integrated Cellular Imaging Core (EICIC) and the Emory Integrated Genomics Core (EIGC) shared resources of Winship Cancer Institute of Emory University, NIH/NCI (award number: P30CA138292), the Canadian Rare Disease Models and Mechanisms Network (RDMM), Citizens United for Research in Epilepsy (339143), the Telethon Undiagnosed Diseases Program (TUDP; GSP15001), the Broad Institute of MIT and Harvard Center for Mendelian Genetics (Broad CMG) funded by the National Human Genome Research Institute, National Eye Institute, and the National Heart, Lung and Blood Institute (UM1-HG008900 and R01-HG009141), and the National Institute for Neurological Disorders and Stroke (U01-NS077303-04S1 and R01-NS058721). The content is solely the responsibility of the authors and does not necessarily reflect the official views of the National Institutes of Health. This study was in part generated within the European Reference Network ITHACA, and uses data shared through RD-Connect, funded by the European Union (FP7/2007-2013, No. 35444).

Additionally, this research was made possible through access to the data and findings generated by the 100,000 Genomes Project. The 100,000 Genomes Project is managed by Genomics England Limited (a wholly owned company of the Department of Health and Social Care). The 100,000 Genomes Project is funded by the National Institute for Health Research and NHS England. The Wellcome Trust, Cancer Research UK and the Medical Research Council have also funded research infrastructure. The 100,000 Genomes Project uses data provided by patients and collected by the National Health Service as part of their care and support.

Competing interests

The authors report no competing interests.

Supplementary material

Supplementary material is available at *Brain* online.

References

1. Forgac M. Vacuolar ATPases: rotary proton pumps in physiology and pathophysiology. *Nat Rev Mol Cell Biol*. Nov 2007;8(11):917-29. doi:10.1038/nrm2272

2. Maxson ME, Grinstein S. The vacuolar-type H(+)-ATPase at a glance - more than a proton pump. *J Cell Sci*. Dec 1 2014;127(Pt 23):4987-93. doi:10.1242/jcs.158550

3. Van Damme T, Gardeitchik T, Mohamed M, et al. Mutations in ATP6V1E1 or ATP6V1A Cause Autosomal-Recessive Cutis Laxa. *Am J Hum Genet*. Feb 2 2017;100(2):216-227. doi:10.1016/j.ajhg.2016.12.010

4. Alazami AM, Al-Qattan SM, Faqeih E, et al. Expanding the clinical and genetic heterogeneity of hereditary disorders of connective tissue. *Hum Genet*. May 2016;135(5):525-540. doi:10.1007/s00439-016-1660-z

5. Kornak U, Reynders E, Dimopoulou A, et al. Impaired glycosylation and cutis laxa caused by mutations in the vesicular H+-ATPase subunit ATP6V0A2. *Nat Genet*. Jan 2008;40(1):32-4. doi:10.1038/ng.2007.45

6. Smith AN, Skaug J, Choate KA, et al. Mutations in ATP6N1B, encoding a new kidney vacuolar proton pump 116-kD subunit, cause recessive distal renal tubular acidosis with preserved hearing. *Nat Genet*. Sep 2000;26(1):71-5. doi:10.1038/79208

7. Karet FE, Finberg KE, Nelson RD, et al. Mutations in the gene encoding B1 subunit of H+-ATPase cause renal tubular acidosis with sensorineural deafness. *Nat Genet*. Jan 1999;21(1):84-90. doi:10.1038/5022

8. Jobst-Schwan T, Klambt V, Tarsio M, et al. Whole exome sequencing identified ATP6V1C2 as a novel candidate gene for recessive distal renal tubular acidosis. *Kidney Int*. Mar 2020;97(3):567-579. doi:10.1016/j.kint.2019.09.026

9. Steward CG. Neurological aspects of osteopetrosis. *Neuropathol Appl Neurobiol*. Apr 2003;29(2):87-97.

10. Frattini A, Orchard PJ, Sobacchi C, et al. Defects in TCIRG1 subunit of the vacuolar proton pump are responsible for a subset of human autosomal recessive osteopetrosis. *Nat Genet*. Jul 2000;25(3):343-6. doi:10.1038/77131

11. Yuan Y, Zhang J, Chang Q, et al. De novo mutation in ATP6V1B2 impairs lysosome acidification and causes dominant deafness-onychodystrophy syndrome. *Cell Res*. Nov 2014;24(11):1370-3. doi:10.1038/cr.2014.77

12. Kortum F, Caputo V, Bauer CK, et al. Mutations in KCNH1 and ATP6V1B2 cause Zimmermann-Laband syndrome. *Nat Genet*. Jun 2015;47(6):661-7. doi:10.1038/ng.3282

13. Zhang Y, Huang H, Zhao G, et al. ATP6V1H Deficiency Impairs Bone Development through Activation of MMP9 and MMP13. *PLoS Genet*. Feb 2017;13(2):e1006481. doi:10.1371/journal.pgen.1006481

14. Fassio A, Esposito A, Kato M, et al. De novo mutations of the ATP6V1A gene cause developmental encephalopathy with epilepsy. *Brain*. Jun 1 2018;141(6):1703-1718. doi:10.1093/brain/awy092

15. Aoto K, Kato M, Akita T, et al. ATP6V0A1 encoding the a1-subunit of the V0 domain of vacuolar H(+)-ATPases is essential for brain development in humans and mice. *Nat Commun*. Apr 8 2021;12(1):2107. doi:10.1038/s41467-021-22389-5

16. Bott LC, Forouhan M, Lieto M, et al. Variants in ATP6V0A1 cause progressive myoclonus epilepsy and developmental and epileptic encephalopathy. *Brain Communications*. 2021;doi:10.1093/braincomms/fcab245

17. Shaw M, Winczewska-Wiktor A, Badura-Stronka M, et al. EXOME REPORT: Novel mutation in ATP6V1B2 segregating with autosomal dominant epilepsy, intellectual disability and mild gingival and nail abnormalities. *Eur J Med Genet*. Oct 23 2019:103799. doi:10.1016/j.ejmg.2019.103799

18. Beauregard-Lacroix E, Pacheco-Cuellar G, Ajeawung NF, et al. DOORS syndrome and a recurrent truncating ATP6V1B2 variant. *Genet Med*. Jan 2021;23(1):149-154. doi:10.1038/s41436-020-00950-9

19. Ramser J, Abidi FE, Burckle CA, et al. A unique exonic splice enhancer mutation in a family with X-linked mental retardation and epilepsy points to a novel role of the renin receptor. *Hum Mol Genet*. Apr 15 2005;14(8):1019-27. doi:10.1093/hmg/ddi094

20. Gupta HV, Vengoechea J, Sahaya K, Virmani T. A splice site mutation in ATP6AP2 causes X-linked intellectual disability, epilepsy, and parkinsonism. *Parkinsonism Relat Disord*. Dec 2015;21(12):1473-5. doi:10.1016/j.parkreldis.2015.10.001

21. Wang L, Wu D, Robinson CV, Wu H, Fu TM. Structures of a Complete Human V-ATPase Reveal Mechanisms of Its Assembly. *Mol Cell*. Nov 5 2020;80(3):501-511 e3. doi:10.1016/j.molcel.2020.09.029

22. Mucha BE, Banka S, Ajeawung NF, et al. A new microdeletion syndrome involving TBC1D24, ATP6V0C, and PDPK1 causes epilepsy, microcephaly, and developmental delay. *Genet Med*. May 2019;21(5):1058-1064. doi:10.1038/s41436-018-0290-3

23. Tinker RJ, Burghel GJ, Garg S, Steggall M, Cuvertino S, Banka S. Haploinsufficiency of ATP6V0C possibly underlies 16p13.3 deletions that cause microcephaly, seizures, and neurodevelopmental disorder. *Am J Med Genet A*. Oct 8 2020;doi:10.1002/ajmg.a.61905

24. Ittiwut C, Poonmaksatit S, Boonsimma P, et al. Novel de novo mutation substantiates ATP6V0C as a gene causing epilepsy with intellectual disability. *Brain Dev*. Mar 2021;43(3):490-494. doi:10.1016/j.braindev.2020.10.016

25. Deciphering Developmental Disorders S. Prevalence and architecture of de novo mutations in developmental disorders. *Nature*. Feb 23 2017;542(7642):433-438. doi:10.1038/nature21062

26. Sobreira N, Schiettecatte F, Valle D, Hamosh A. GeneMatcher: a matching tool for connecting investigators with an interest in the same gene. *Hum Mutat*. Oct 2015;36(10):928-30. doi:10.1002/humu.22844

27. Investigators GPP, Smedley D, Smith KR, et al. 100,000 Genomes Pilot on Rare-Disease Diagnosis in Health Care - Preliminary Report. *N Engl J Med*. Nov 11 2021;385(20):1868-1880. doi:10.1056/NEJMoa2035790

28. Carvill GL, Weckhuysen S, McMahon JM, et al. GABRA1 and STXBP1: novel genetic causes of Dravet syndrome. *Neurology*. Apr 8 2014;82(14):1245-53. doi:10.1212/WNL.0000000000000291

29. Jay JJ, Brouwer C. Lollipops in the Clinic: Information Dense Mutation Plots for Precision Medicine. *PLoS One*. 2016;11(8):e0160519. doi:10.1371/journal.pone.0160519

30. Butler KM, Moody OA, Schuler E, et al. De novo variants in GABRA2 and GABRA5 alter receptor function and contribute to early-onset epilepsy. *Brain*. Aug 1 2018;141(8):2392-2405. doi:10.1093/brain/awy171

31. Karczewski KJ, Francioli LC, Tiao G, et al. The mutational constraint spectrum quantified from variation in 141,456 humans. *Nature*. May 2020;581(7809):434-443. doi:10.1038/s41586-020-2308-7

32. Traynelis J, Silk M, Wang Q, et al. Optimizing genomic medicine in epilepsy through a gene-customized approach to missense variant interpretation. *Genome Res*. Oct 2017;27(10):1715-1729. doi:10.1101/gr.226589.117

33. Marley R, Baines RA. Increased persistent Na+ current contributes to seizure in the slamdance bang-sensitive Drosophila mutant. *J Neurophysiol*. Jul 2011;106(1):18-29. doi:10.1152/jn.00808.2010

34. Berman H, Henrick K, Nakamura H, Markley JL. The worldwide Protein Data Bank (wwPDB): ensuring a single, uniform archive of PDB data. *Nucleic Acids Res*. Jan 2007;35(Database issue):D301-3. doi:10.1093/nar/gkl971

35. Guex N, Peitsch MC. SWISS-MODEL and the Swiss-PdbViewer: an environment for comparative protein modeling. *Electrophoresis*. Dec 1997;18(15):2714-23. doi:10.1002/elps.1150181505

36. Green MR, Sambrook J, Sambrook J. *Molecular cloning : a laboratory manual*. 4th ed. Cold Spring Harbor Laboratory Press; 2012.

37. Sikorski RS, Hieter P. A system of shuttle vectors and yeast host strains designed for efficient manipulation of DNA in Saccharomyces cerevisiae. *Genetics*. May 1989;122(1):19-27.

38. Perzov N, Padler-Karavani V, Nelson H, Nelson N. Characterization of yeast V-ATPase mutants lacking Vph1p or Stv1p and the effect on endocytosis. *J Exp Biol*. May 2002;205(Pt 9):1209-19.

39. Sprouffske K, Wagner A. Growthcurver: an R package for obtaining interpretable metrics from microbial growth curves. *BMC Bioinformatics*. Apr 19 2016;17:172. doi:10.1186/s12859-016-1016-7

40. Restif C, Ibáñez-Ventoso C, Vora MM, Guo S, Metaxas D, Driscoll M. CeleST: Computer Vision Software for Quantitative Analysis of C. elegans Swim Behavior Reveals Novel Features of Locomotion. *PLOS Computational Biology*. 2014;10(7):e1003702. doi:10.1371/journal.pcbi.1003702

41. Kircher M, Witten DM, Jain P, O'Roak BJ, Cooper GM, Shendure J. A general framework for estimating the relative pathogenicity of human genetic variants. *Nat Genet*. Mar 2014;46(3):310-5. doi:10.1038/ng.2892

42. Richards S, Aziz N, Bale S, et al. Standards and guidelines for the interpretation of sequence variants: a joint consensus recommendation of the American College of Medical Genetics and Genomics and the Association for Molecular Pathology. *Genet Med*. May 2015;17(5):405-24. doi:10.1038/gim.2015.30

43. Yamamoto GL, Aguena M, Gos M, et al. Rare variants in SOS2 and LZTR1 are associated with Noonan syndrome. *J Med Genet*. Jun 2015;52(6):413-21. doi:10.1136/jmedgenet-2015-103018

44. de Goede C, Yue WW, Yan G, et al. Role of reverse phenotyping in interpretation of next generation sequencing data and a review of INPP5E related disorders. *Eur J Paediatr Neurol*. Mar 2016;20(2):286-295. doi:10.1016/j.ejpn.2015.11.012

45. Bockelmann S, Menche D, Rudolph S, et al. Archazolid A binds to the equatorial region of the c-ring of the vacuolar H+-ATPase. *J Biol Chem*. Dec 3 2010;285(49):38304-14. doi:10.1074/jbc.M110.137539

46. Kawasaki-Nishi S, Nishi T, Forgac M. Interacting helical surfaces of the transmembrane segments of subunits a and c' of the yeast V-ATPase defined by disulfide-mediated cross-linking. *J Biol Chem*. Oct 24 2003;278(43):41908-13. doi:10.1074/jbc.M308026200

47. Nelson H, Nelson N. Disruption of genes encoding subunits of yeast vacuolar H(+)-ATPase causes conditional lethality. *Proc Natl Acad Sci U S A*. May 1990;87(9):3503-7.

48. Su Y, Blake-Palmer KG, Sorrell S, et al. Human H+ATPase a4 subunit mutations causing renal tubular acidosis reveal a role for interaction with phosphofructokinase-1. *Am J Physiol Renal Physiol*. Oct 2008;295(4):F950-8. doi:10.1152/ajprenal.90258.2008

49. Zirngibl RA, Wang A, Yao Y, et al. Novel c.G630A TCIRG1 mutation causes aberrant splicing resulting in an unusually mild form of autosomal recessive osteopetrosis. *J Cell Biochem*. Oct 2019;120(10):17180-17193. doi:10.1002/jcb.28979

50. Ochotny N, Van Vliet A, Chan N, et al. Effects of human a3 and a4 mutations that result in osteopetrosis and distal renal tubular acidosis on yeast V-ATPase expression and activity. *J Biol Chem*. Sep 8 2006;281(36):26102-11. doi:10.1074/jbc.M601118200

51. Ohya Y, Umemoto N, Tanida I, Ohta A, Iida H, Anraku Y. Calcium-sensitive cls mutants of Saccharomyces cerevisiae showing a Pet- phenotype are ascribable to defects of vacuolar membrane H(+)-ATPase activity. *J Biol Chem*. Jul 25 1991;266(21):13971-7.

52. Vaccaro A, Tauffenberger A, Aggad D, Rouleau G, Drapeau P, Parker JA. Mutant TDP-43 and FUS cause age-dependent paralysis and neurodegeneration in C. elegans. *PLoS One*. 2012;7(2):e31321. doi:10.1371/journal.pone.0031321

53. Mahoney TR, Luo S, Nonet ML. Analysis of synaptic transmission in Caenorhabditis elegans using an aldicarb-sensitivity assay. *Nat Protoc*. 2006;1(4):1772-7. doi:10.1038/nprot.2006.281

54. Vashlishan AB, Madison JM, Dybbs M, et al. An RNAi screen identifies genes that regulate GABA synapses. *Neuron*. May 8 2008;58(3):346-61. doi:10.1016/j.neuron.2008.02.019

55. Hawasli AH, Saifee O, Liu C, Nonet ML, Crowder CM. Resistance to volatile anesthetics by mutations enhancing excitatory neurotransmitter release in Caenorhabditis elegans. *Genetics*. Oct 2004;168(2):831-43. doi:10.1534/genetics.104.030502

56. Saifee O, Wei L, Nonet ML. The Caenorhabditis elegans unc-64 locus encodes a syntaxin that interacts genetically with synaptobrevin. *Mol Biol Cell*. Jun 1998;9(6):1235-52. doi:10.1091/mbc.9.6.1235

57. Acuna-Hidalgo R, Bo T, Kwint MP, et al. Post-zygotic Point Mutations Are an Underrecognized Source of De Novo Genomic Variation. *Am J Hum Genet*. Jul 2 2015;97(1):67-74. doi:10.1016/j.ajhg.2015.05.008

58. Cook CB, Armstrong L, Boerkoel CF, et al. Somatic mosaicism detected by genome-wide sequencing in 500 parent-child trios with suspected genetic disease: Clinical and genetic counseling implications. *Cold Spring Harbor molecular case studies*. Oct 25 2021;doi:10.1101/mcs.a006125

59. Dyle MC, Kolakada D, Cortazar MA, Jagannathan S. How to get away with nonsense: Mechanisms and consequences of escape from nonsense-mediated RNA decay. *Wiley Interdiscip Rev RNA*. Jan 2020;11(1):e1560. doi:10.1002/wrna.1560

60. Bowman BJ, McCall ME, Baertsch R, Bowman EJ. A model for the proteolipid ring and bafilomycin/concanamycin-binding site in the vacuolar ATPase of Neurospora crassa. *J Biol Chem*. Oct 20 2006;281(42):31885-93. doi:10.1074/jbc.M605532200

61. McIntire SL, Reimer RJ, Schuske K, Edwards RH, Jorgensen EM. Identification and characterization of the vesicular GABA transporter. *Nature*. Oct 23 1997;389(6653):870-6. doi:10.1038/39908

62. Bellocchio EE, Reimer RJ, Fremeau RT, Jr., Edwards RH. Uptake of glutamate into synaptic vesicles by an inorganic phosphate transporter. *Science*. Aug 11 2000;289(5481):957-60. doi:10.1126/science.289.5481.957

63. Morel N, Poea-Guyon S. The membrane domain of vacuolar H(+)ATPase: a crucial player in neurotransmitter exocytotic release. *Cell Mol Life Sci*. Jul 2015;72(13):2561-73. doi:10.1007/s00018-015-1886-2

64. Peters C, Bayer MJ, Buhler S, Andersen JS, Mann M, Mayer A. Trans-complex formation by proteolipid channels in the terminal phase of membrane fusion. *Nature*. Feb 1 2001;409(6820):581-8. doi:10.1038/35054500

65. Wang D, Epstein D, Khalaf O, et al. Ca2+-Calmodulin regulates SNARE assembly and spontaneous neurotransmitter release via v-ATPase subunit V0a1. *J Cell Biol*. Apr 14 2014;205(1):21-31. doi:10.1083/jcb.201312109

66. Maxfield FR, McGraw TE. Endocytic recycling. *Nat Rev Mol Cell Biol*. Feb 2004;5(2):121-32. doi:10.1038/nrm1315

67. Presley JF, Mayor S, McGraw TE, Dunn KW, Maxfield FR. Bafilomycin A1 treatment retards transferrin receptor recycling more than bulk membrane recycling. *J Biol Chem*. May 23 1997;272(21):13929-36. doi:10.1074/jbc.272.21.13929

68. Zhang X, Bao L, Ma GQ. Sorting of neuropeptides and neuropeptide receptors into secretory pathways. *Prog Neurobiol*. Feb 9 2010;90(2):276-83. doi:10.1016/j.pneurobio.2009.10.011

69. Khayat W, Hackett A, Shaw M, et al. A recurrent missense variant in SLC9A7 causes nonsyndromic X-linked intellectual disability with alteration of Golgi acidification and aberrant glycosylation. *Hum Mol Genet*. Feb 15 2019;28(4):598-614. doi:10.1093/hmg/ddy371

70. Sobota JA, Back N, Eipper BA, Mains RE. Inhibitors of the V0 subunit of the vacuolar H+-ATPase prevent segregation of lysosomal- and secretory-pathway proteins. *J Cell Sci*. Oct 1 2009;122(Pt 19):3542-53. doi:10.1242/jcs.034298

71. Nakamura N, Matsuura A, Wada Y, Ohsumi Y. Acidification of vacuoles is required for autophagic degradation in the yeast, Saccharomyces cerevisiae. *J Biochem*. Feb 1997;121(2):338-44. doi:10.1093/oxfordjournals.jbchem.a021592

72. Fassio A, Falace A, Esposito A, Aprile D, Guerrini R, Benfenati F. Emerging Role of the Autophagy/Lysosomal Degradative Pathway in Neurodevelopmental Disorders With Epilepsy. *Front Cell Neurosci*. 2020;14:39. doi:10.3389/fncel.2020.00039

73. Saha S, Panigrahi DP, Patil S, Bhutia SK. Autophagy in health and disease: A comprehensive review. *Biomed Pharmacother*. Aug 2018;104:485-495. doi:10.1016/j.biopha.2018.05.007

74. Fagerberg L, Hallstrom BM, Oksvold P, et al. Analysis of the human tissue-specific expression by genome-wide integration of transcriptomics and antibody-based proteomics. *Mol Cell Proteomics*. Feb 2014;13(2):397-406. doi:10.1074/mcp.M113.035600

Figure legends

Figure 1 V-ATPase Structure. The peripheral domain (V_1, uppercase letters, in grey) is the site of ATP binding and hydrolysis. The integral domain (V_0, lowercase letters, in purple, red, blue, and yellow) transports protons across membranes. The c-ring (red) is composed of 9 c-subunits (encoded by *ATP6V0C*) and 1 c″-subunit (encoded by *ATP6V0B,* not shown) and rotates after ATP hydrolysis to bring protons to ATP6V0A (blue). ATP6V0A possess two hemi-channels and a buried arginine residue (p.R735) which are required along with p.E139 in ATP6V0C for proton translocation.[1]

Figure 2 Location and Conservation of ATP6V0C Variants. (**A**) Exon/intron structure of *ATP6V0C*. Boxes represent exons with black denoting coding regions. Scale bar provided represents 100bp length. (**B**) Protein alignment showing conservation of affected residues (highlighted in yellow). Glutamate residue (p.E139) required for proton transport is bolded. The following protein sequences were used in the alignments: *H. sapiens*, NP_001685.1; *M. musculus*, NP_001348461.1; *D. rerio*, NP_991117.7; *D. melanogaster*, NP_476801.1; *C. elegans*, NP_499166.1; *S. cerevisiae*, NP_010887.3. (**C**) Lollipop plot showing the transmembrane structure (green) and location of variants throughout ATP6V0C. Patient missense variants are indicated with red. Missense (blue) and synonymous (grey) variants observed in gnomAD are shown. Based on UniProt accession P27449. There is a significant enrichment of patient variants in TM4 (p = 0.006, Fisher's Exact test). (**D**) Plot showing tolerance of missense variants across ATP6V0C. Missense tolerance ratio (MTR) calculated using 21 codon window sizes. A MTR score of < 1 indicates intolerance to missense variation. Dashed lines on the plot denote ATP6V0C-specific MTRs: green = 5^{th} percentile, yellow = 25^{th} percentile, and black = 50^{th} percentile.

Figure 3 Knockdown of the *Drosophila* Ortholog of *ATP6V0C* Increases Seizure Duration. (**A**) Pan-neuronal (elaV-GAL4) RNAi-mediated knockdown of Dmel\Vha16-3 (CG32090) using RNAi (elaV>102067 RNAi) is sufficient to increase the recovery time (RT) of third instar larvae to electroshock-induced seizure. Controls expressed GFP RNAi via elaV-GAL4 (elaV>GFP RNAi) or the RNAi (102067) without a driver (102067 RNAi). (**B**) Seizure-induction due to expression of 102067 RNAi is preferentially rescued by pre-treatment of larvae with levetiracetam (LEV) or topiramate (TOP). Lamotrigine (LAM) and valproate (VAL) were also effective, but not phenytoin (PHY). RT was normalized to a

vehicle (DMSO) only control. Data shown as mean ± SEM. One-way ANOVA with post-hoc comparison (Dunnett's); *$p < 0.05$, **$p < 0.01$, ***$p < 0.001$, ****$p < 0.0001$.

Figure 4 Molecular Modeling of Patient and gnomAD Variants. (**A**) Structure of part of the V_0 region of human V-ATPase (PDB: 6wlw).[21] Sites of patient (purple) and gnomAD (green) variants are shown superposed on ribbon backbone for two ATP6V0C subunits (gold), one next to the ATP6V0A subunit (cyan) and one on the opposite side of the c-ring. The back part of the c-ring is filled with grey, and the front part has been omitted for clarity. (**B**) Isolated view of the interaction between ATP6V0C variants and ATP6V0A. The functional amino acid p.E139 is also displayed (pink).

Figure 5 Patient Variants Show Reduced V-ATPase Function. (**A**) Quantification of average fluorescent intensity for each variant in the LysoSensor assay. Variants are grouped based on their location within or proximity to the nearest transmembrane (TM) domain. Data was normalized with mean of wild type as 100% (denoted by dotted line) and mean of empty vector as 0%. Data shown as mean ± SEM (n = 71-132 cells/variant). Box and whisker plot of this data is presented in **Supplemental Fig 4**. (**B-E**) Growth curves of *vma3Δ S. cerevisiae* expressing patient or gnomAD variants when grown in YPD, pH 5.5 with 5mM $CaCl_2$. In all panels, wild type is shown in black and the empty vector in grey. Mean of 9 replicates per construct is shown with error bars omitted for clarity. Variants are grouped based on their location within or proximity to the nearest TM domain. (**F**) eAUC was calculated using Growthcurver.[39] Data was normalized within each plate with wild type as 100% (denoted by dotted line) and empty vector as 0% and is shown as mean ± SEM. A one sample t-test to a hypothetical mean of 100 was conducted with a Bonferroni correction (adjusted α level = 0.0003125). **$p < 0.01$, ***$p < 0.001$, $^{\#}p < 0.0001$.

Figure 6 Expression of patient variants in *C. elegans* exacerbate motor dysfunction and reduce lifespan. (**A-B**) WormLab analysis of body length and size at day 1 of adulthood. All mutants are shorter and smaller than N2 controls. (**C-D**) Automated analysis of worm movement in liquid culture by WormTracker software. (**C**) In physiological M9 solution, all mutants show no motor deficits. (**D**) In presence of 350mM NaCl concentration the p.G63A ($p < 0.0001$) and p.F137L ($p < 0.0062$) mutants show reduced movement scores in liquid culture over 270 minutes. Reduced movement was also observed with the p.L150F variant, but this difference was not statistically significant (p = 0.0869). (**E**) All mutant strains

showed increased paralysis over 14 days compared to N2 controls (n = 313-317 / strain, p < 0.0001). (**F-G**) In presence of osmotic stress (200 or 300mM NaCl) the paralysis phenotype is exacerbated, leading to almost 100% paralysis after 8 days for the p.G63A strain (n = 246 – 260 / strain, p < 0.0001). (**H**) All mutant strains exhibited reduced lifespan compared to N2 controls (n = 219 – 233 / strain, p < 0.0001). (**I-J**) All mutant strains have reduced lifespans in presence of osmotic stress compared to N2 controls. (200mM NaCl: n = 182 – 228 / strain. 300mM, p < 0.0001) (300mM NaCl: n = 200 – 244 / strain, p < 0.0001). *p < 0.05, **p < 0.01, ***p < 0.001, ****p < 0.0001 compared to N2 controls.

Figure 7 Patient mutations cause increased uncoordinated movement and neuronal signaling dysfunction in *C. elegans*. (**A-C**) Analysis of fine motor movement of worms after 30 minutes in 500mM NaCl liquid culture. Mutants show increased activity index and wave initiation (A&B), but swimming speed was not significantly altered (**C**). (**D**) Synaptic transmission was evaluated by exposing day 1 adult worms to aldicarb. Worms were scored over a 2-hour period for paralysis. All mutants were hypersensitive to aldicarb treatment compared to N2 worms (n = 236 – 296 / strain). *p < 0.05, **p < 0.01, ***p < 0.001, ****p < 0.0001 compared to N2 controls.

Table 1 Clinical Presentation of Patients with *ATP6V0C* Variants

Patient	Variant[a]	CADD Score[b]	Inheritance	Seizures (Age at Onset)	Seizure Types	Developmental Delay	Intellectual Disability[c]
1[d]	c.85G>A; p.G29S	26.2	*de novo*	NA	NA	NA	NA
2[e]	c.134_135delCT; p.(S45CfsTer37)	NA	*de novo*	Yes (7mo)	GTCS, At, FDS, Myo, T	NA	Severe, with regression
3	c.143G>C; p.R48P	27.2	*de novo*	Yes (18mo)	NA	Yes, motor and speech	NA
4	c.158T>G; p.M53R	25.9	*de novo,* mosaic	No	NA	Yes	Too young for evaluation
5[f]	c.172C>G; p.P58A	23.1	NA	Yes	Cryptogenic focal	Yes, psychomotor	NA
6	c.188G>C; p.G63A	23.9	*de novo*	Yes (8mo)	Infantile spasms, GTCS, At, Myo	Yes, non-verbal	Severe
7	c.214delG; p.(V72WfsTer9)	NA	*de novo*	Yes	Infantile spasms	Yes	Too young for evaluation
8	c.220G>T; p.V74F	26	*de novo*	Yes (12mo)	GTCS, Ab, FOA	Yes, motor and speech	Severe
9	c.283G>A; p.A95T	26.2	*de novo*, mosaic	Yes (10mo)	GTCS, FOA, Febrile	Yes, regression to non-verbal	Profound
10	c.283G>C; p.A95P	24.6	*de novo*	Yes (10mo)	GTCS, staring	Yes, motor and non-verbal	Too young for evaluation
11	c.284C>T; p.A95V	23.7	*de novo*	Yes (5mo)	Febrile, Ab, Myo, T (nocturnal)	No	Moderate
12[d]	c.294C>A; p.S98R	13.2	*de novo*	NA	NA	NA	NA
13[g]	c.340_355del16; p.(D115AfsTer12)	NA	*de novo*	Yes (16mo)	Focal with secondary generalization	Yes, speaks only in short sentences	Yes
14	c.352_362delins; p.(V118HfsTer19)	NA	*de novo*	Yes (30mo)	GTCS, focal to bilateral TCS, Ab, FIA	Yes, motor and speech	Mild, regression in adulthood
15	c.395T>A; p.I132N	25.3	*de novo*, mosaic	Yes (12yr)	NA	Yes	Yes
16	c.409T>C; p.F137L	25.2	*de novo*	Yes (13mo)	GTCS, Myo, At, FOA	Yes, motor and non-verbal	Profound
17	c.412G>C; p.A138P	25.5	*de novo*	NA	TCS	Yes	NA
18	c.412G>C; p.A138P	25.5	*de novo*	Yes (6mo)	GTCS, multifocal	Yes, motor and speech	Too young for evaluation
19	c.425G>A; p.G142D	24.7	*de novo*, mosaic	No	NA	Yes, motor and non-verbal	Too young for evaluation
20	c.440T>C; p.I147T	23.3	*de novo*	Yes	NA	Yes, speech	Profound
21	c.445G>A; p.A149T	24.3	*de novo*	Yes (38mo)	Febrile, TCS, Myo, Ab	Yes, motor and speech	Mild
22	c.445G>A; p.A149T	24.3	*de novo*	Yes (6mo)	GTCS, At, TCS	Yes, motor and speech	Mild
23[d]	c.448C>T; p.L150F	25.1	NA	NA	NA	NA	NA
24	c.448C>T; p.L150F	25.1	*de novo*	Yes (6mo)	Infantile flexor spasms, T (w/ asymmetrical limb stiffening)	Yes, motor and speech	Profound
25	c.448C>T; p.L150F	25.1	*de novo*	Yes (6yr)	GTCS	Yes, motor and speech	Severe
26	c.449T>C; p.L150P	24.7	*de novo*	Yes (18mo)	Febrile, GTCS, T, At, Ab	Yes, fine motor	Mild
27[h]	c.467A>T; p.(Ter156LeuextTer35)	NA	*de novo*	Yes (24mo)	GTCS, TCS, At, afebrile	No	Yes, with regression

Ab = absence, At = atonic, FDS = focal dyscognitive seizures, FOA = Focal onset aware (Partial), FIA = Focal impaired aware, GTCS = Generalized Tonic-clonic seizures, Myo = Myoclonic, NA = not available, T = Tonic, TCS = Tonic-clonic seizures.

[a]Based on reference sequence NM_001694.4.

[b]Scores obtained using CADD GRCh37-v1.6.

[c]Intellectual Disability can usually be first assessed at 5 years of age.

[d]Patients 1, 12, and 23 have severe neurodeveopmental diseases but detailed clinical information was unavailable.

[e]Previously published as Patient T1911 in Carvill *et al.*[28]

[f]ClinVar Variant: VCV000870676.

[g]Previously published as DDD4K.04123 in DDD study.[25]

[h]Previously published in Ittiwut *et al.*[24]

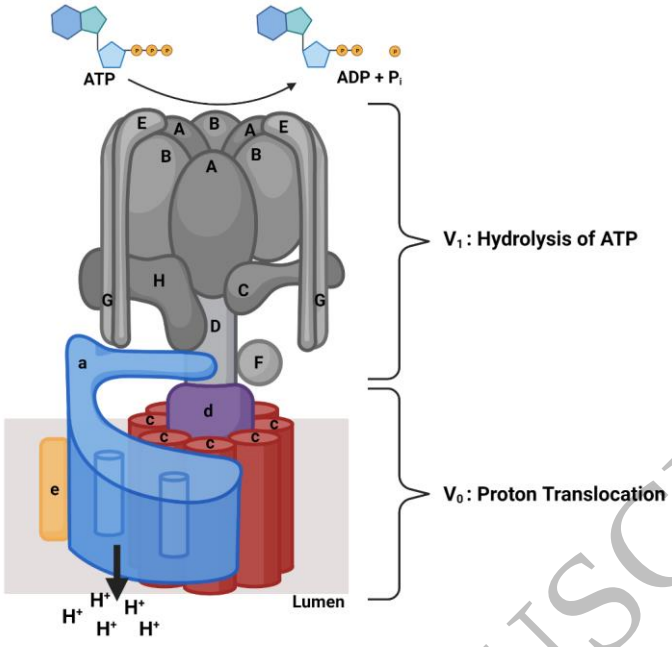

Figure 1
90x85 mm (.49 x DPI)

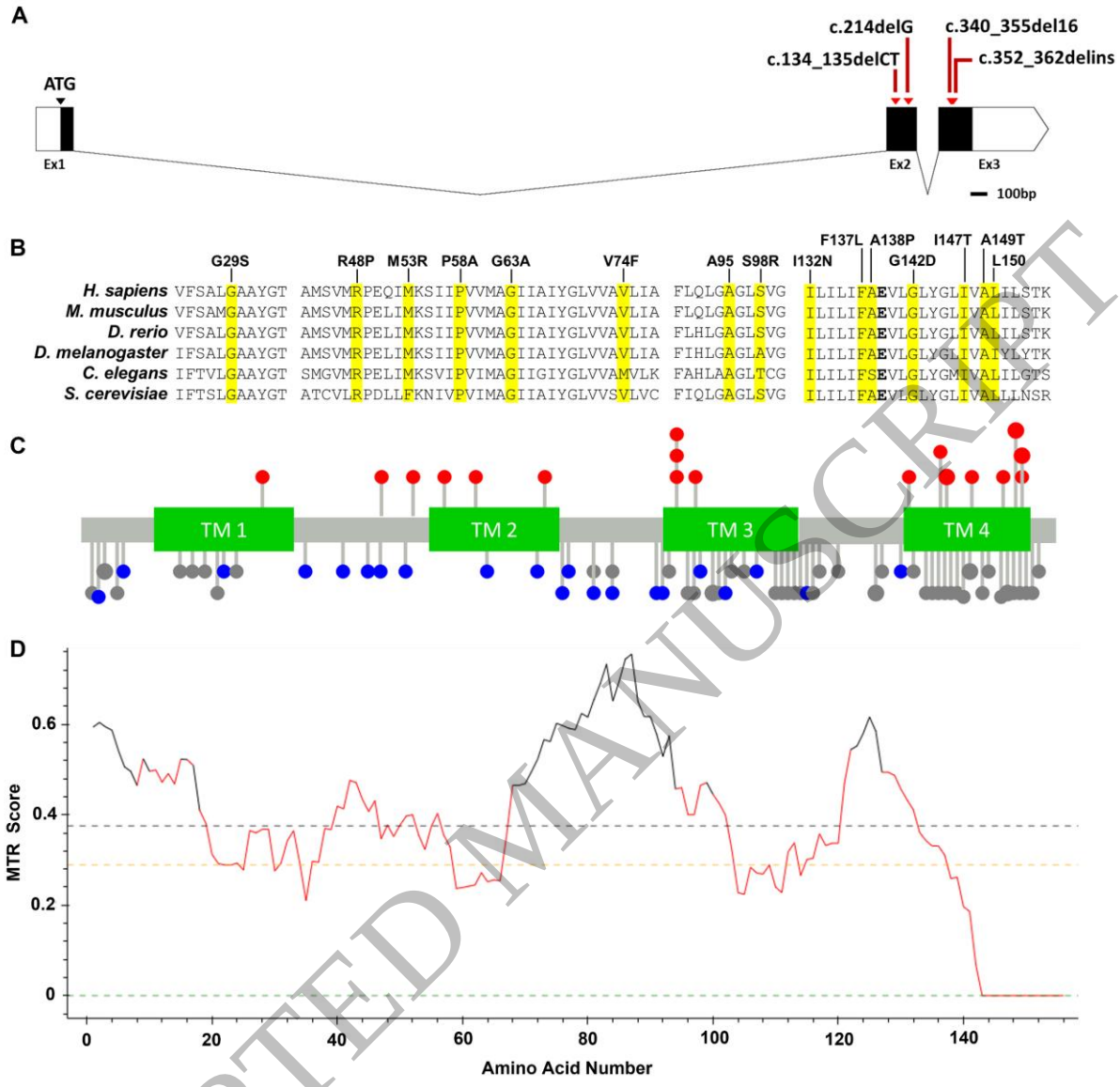

Figure 2
159x154 mm (.49 x DPI)

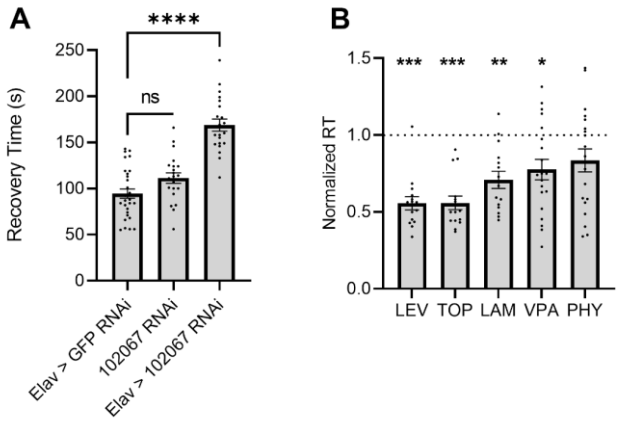

Figure 3
90x59 mm (.49 x DPI)

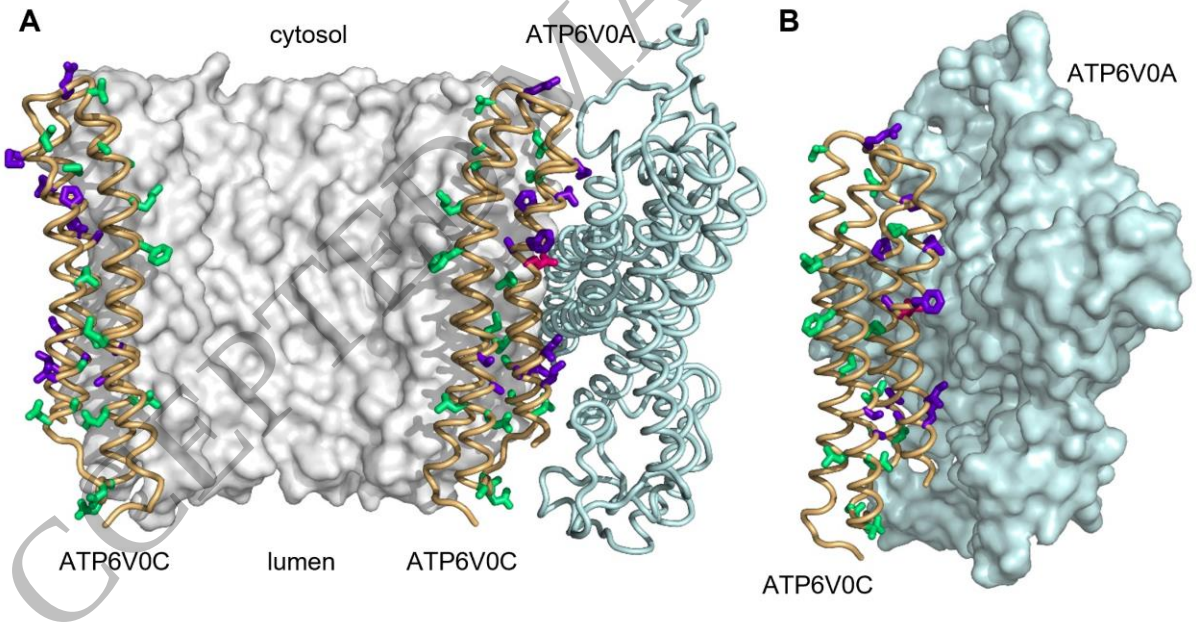

Figure 4
159x81 mm (.49 x DPI)

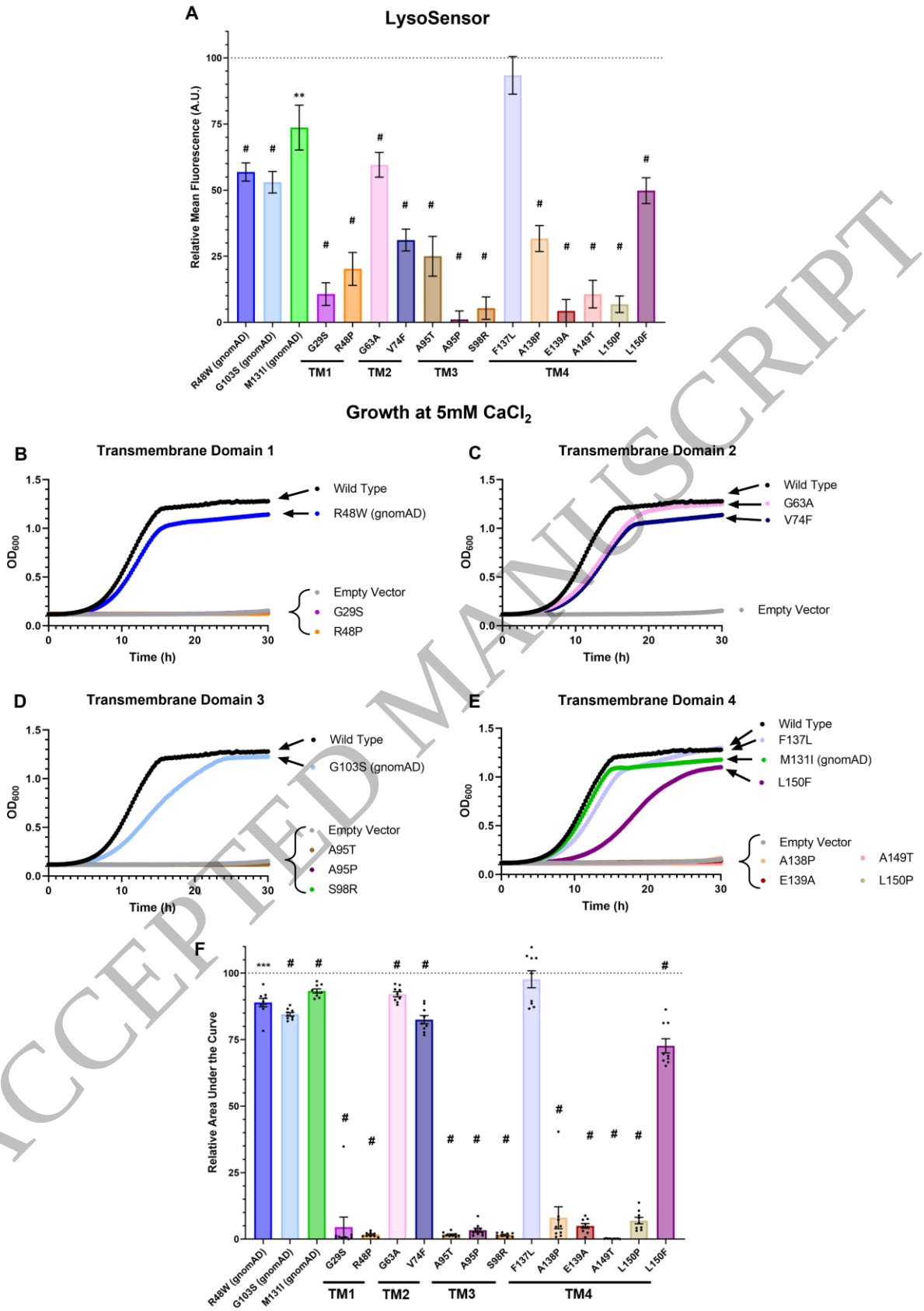

Figure 5
159x225 mm (.49 x DPI)

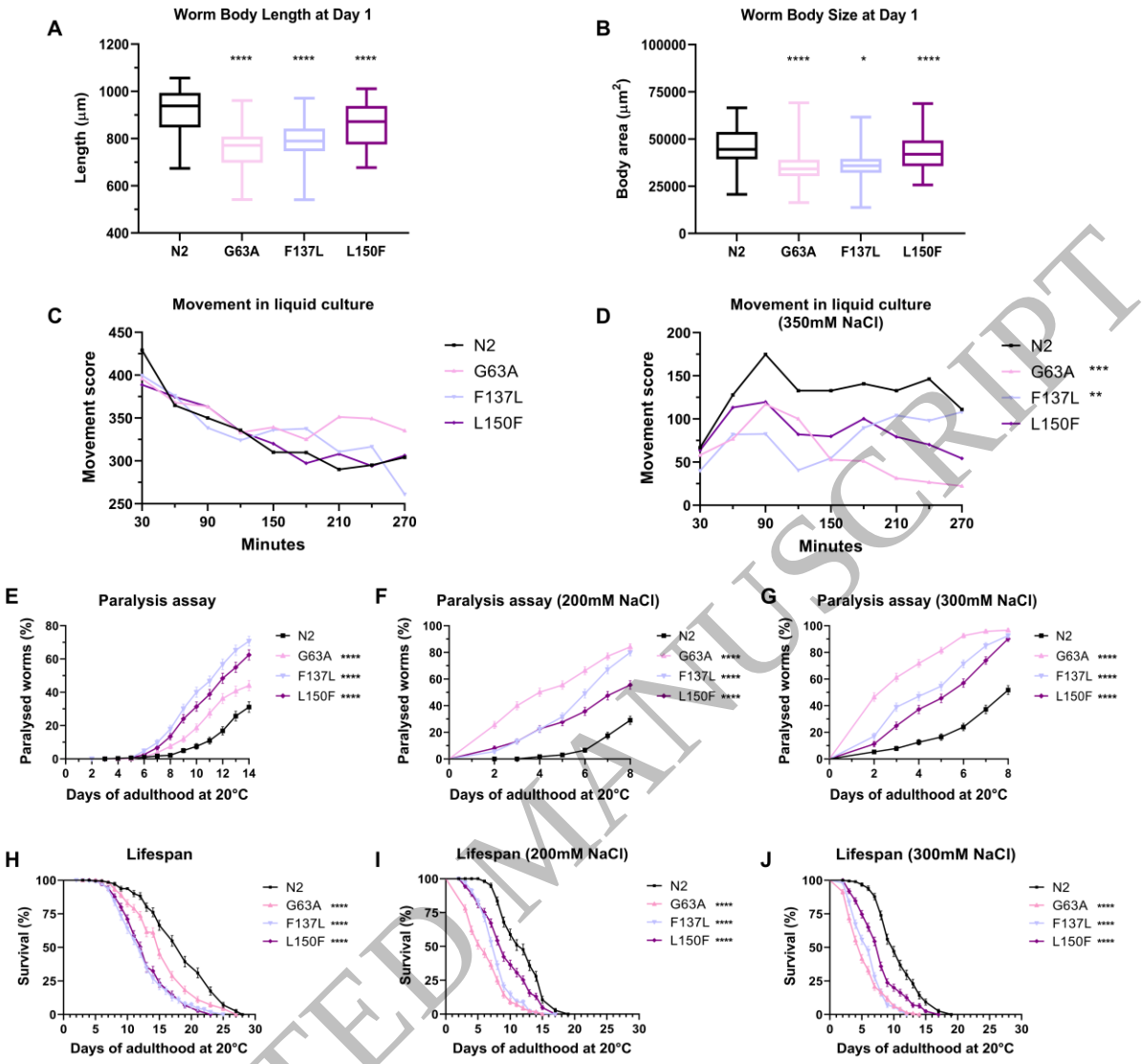

Figure 6
159x152 mm (.49 x DPI)

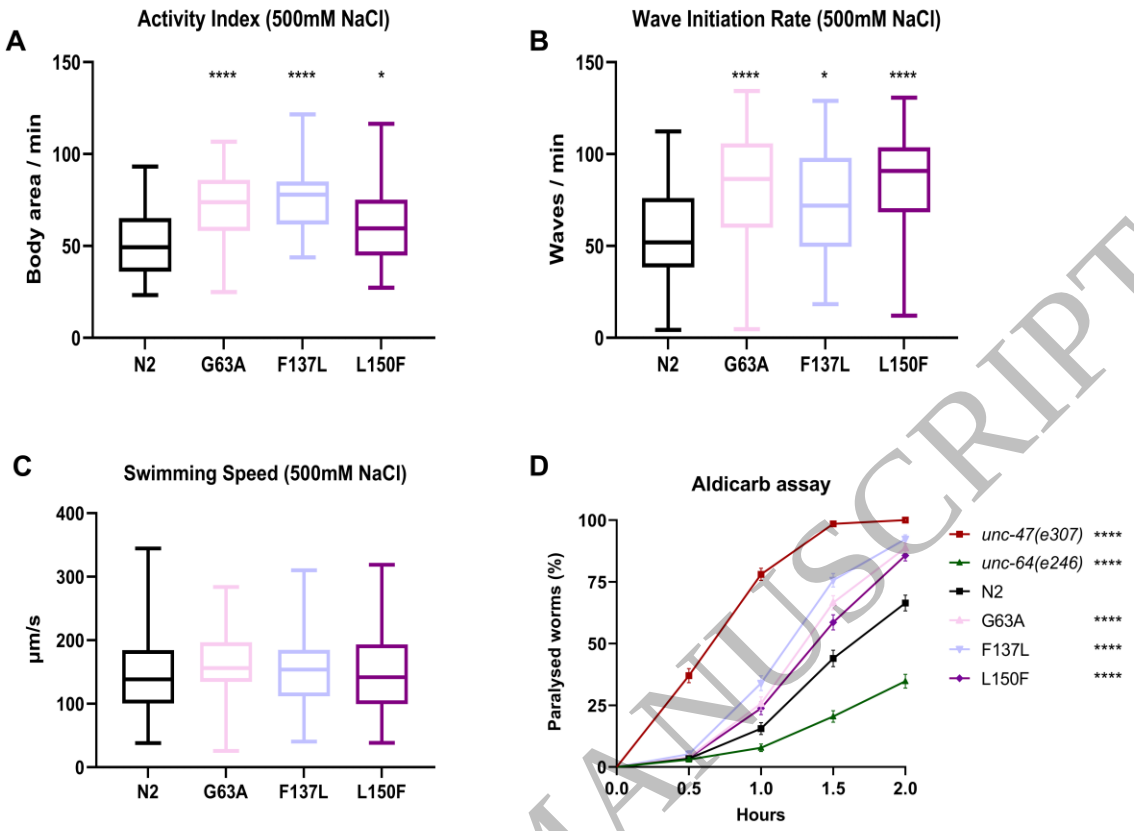

Figure 7
159x117 mm (.49 x DPI)